applied sciences

MDPI

Article

AE Feature-Driven Evaluation of Rock Brittleness and the Mechanism of Damage–Fracture Evolution

Xinnan Cui [1], Chong Chen [2], Li Bi [3] and Chunping Wu [4,*]

[1] National School of Elite Engineering USTB, University of Science and Technology Beijing, Beijing 100083, China; chester_tsui@ustb.edu.cn
[2] Ansteel Beijing Research Institute Co., Ltd., Beijing 102211, China; chenchong.2018@tsinghua.org.cn
[3] Ansteel Cornerstone Mining Co., Ltd., Anshan 114047, China; bili_mining@163.com
[4] School of Resources and Safety Engineering, University of Science and Technology Beijing, Beijing 100083, China
* Correspondence: clydewu@ustb.edu.cn

Abstract

Ultra-large underground metal mines often have complex surrounding rock structures, making traditional assessment methods inadequate for warning against the sudden failure of highly brittle rock masses. To accurately identify high-risk rock layers, this study combines Brazilian splitting tests with acoustic emission (AE) monitoring on four typical surrounding rocks. A normalized damage–stress brittleness coefficient (NDBC) is proposed, and Gaussian mixture model (GMM) clustering is employed to analyze crack evolution mechanisms. Different from conventional brittleness indexes merely based on mechanical parameters, the proposed NDBC characterizes rock brittleness from the perspective of progressive damage evolution driven by acoustic emission microfracture information, providing a dynamic evaluation basis for sudden instability in highly brittle rock masses. The GMM clustering automatically identifies crack features and accurately quantifies the transition from tensile peak to increasing shear during the failure process. The research shows that: (1) AE characteristics during the failure stage are manifested as medium- to high-frequency signals caused by small-scale cracks. (2) Siliceous limestone exhibits extremely high brittleness (NDBC of 0.07) and sudden failure due to the difficulty of microcrack propagation, posing a greater risk of instability and potential overall collapse during mining; in contrast, granite (NDBC of 0.23) is more ductile, showing progressive damage accumulation. (3) Initial rock splitting failure is primarily tensile cracking, with shear cracking increasing as failure approaches, transitioning the failure mechanism to a tensile–shear composite mode. Therefore, establishing a differentiated monitoring and prevention system based on AE main frequency identification and GMM analysis, designating siliceous limestone surrounding rock areas as key prevention zones, can effectively reduce the risk of sudden instability and ensure safe mining operations.

Keywords: rock brittleness evaluation; crack evolution mechanism; acoustic emission characteristics; GMM clustering

Check for updates

Academic Editor: Nikolaos Koukouzas

Received: 3 April 2026
Revised: 27 April 2026
Accepted: 28 April 2026
Published: 1 May 2026

Copyright: © 2026 by the authors. Licensee MDPI, Basel, Switzerland. This article is an open access article distributed under the terms and conditions of the Creative Commons Attribution (CC BY) license.

1. Introduction

The surrounding rock of ultra-large underground metal mines exhibits significant lithological heterogeneity and structural complexity. High-brittleness rock masses are prone to sudden instability during mining, which seriously threatens the safe production of mines [1]. As a key mechanical property of rock, brittleness determines that high-brittleness

rocks tend to show sudden and violent failure characteristics when the stress reaches the limit [2], and such failures often lack obvious precursors, making it difficult for traditional monitoring methods to achieve effective early warning. Essentially, surrounding rock instability is the result of the entire evolutionary process of internal cracks from initiation and propagation to coalescence. The coupling effect of high in situ stress and mining disturbance makes this process exhibit significant nonlinear characteristics, and traditional empirical judgments or local monitoring struggles to fully capture its dynamic laws [3].

During the loading process, the generation, propagation and coalescence of internal cracks will trigger the instantaneous release of energy, thereby generating acoustic emission (AE) signals. Basic characteristics of AE such as count, duration, rise time, energy, and amplitude, as well as RA value, AF value, and FR value derived from these parameters, are closely related to the internal failure mechanism of rock [4–6]. AE technology provides a dynamic and real-time monitoring method for the study of rock mass failure mechanisms by capturing elastic waves released during the initiation, propagation and coalescence of internal rock cracks. In recent years, rock mechanics research based on AE characteristics has made significant progress in the field of mining engineering. For example, Guo [7] explored the fracture evolution and mechanical mechanism of rock mass under anchorage by monitoring displacement and AE signals. However, the quantitative correlation model between AE parameters and the critical state of rock mass instability in existing research is still imperfect, which restricts the accuracy of disaster early warning. Therefore, in-depth study of the AE characteristics of rocks, establishment of rock brittleness evaluation methods and crack evolution monitoring systems, revelation of the critical transition mechanism from “stable bearing” to “sudden instability”, and restoration of the dynamic path of cracks from “microdamage” to “macroinstability” have important theoretical value for preventing engineering disasters such as mine collapse and tunnel rockburst.

Existing brittleness evaluation indicators have obvious limitations: static indicators based on elastic parameters [8] and strength characteristics [9] often lead to contradictory evaluation results due to differences in test conditions and parameter selection. More importantly, such indicators struggle to reflect the dynamic process of damage accumulation. When rock is loaded, cracks in brittle rock tend to nucleate and propagate rapidly, releasing a large amount of energy in a short time, which is manifested as a high AE count [10]; while in the deformation process of ductile rock, energy release is relatively slow and dispersed, with a low AE count. Based on this, some studies use cumulative hits to define the damage variable of rock, that is, by calculating the ratio of the current cumulative count to the cumulative count at the time of failure [11], but this method has two limitations: first, the total numbers of AE hits of different lithologies vary significantly, making them difficult to compare horizontally; second, it does not consider the impact of stress level on damage development. Therefore, this study proposes a normalized damage–stress brittleness coefficient (NDBC), which eliminates the differences in sample size and loading conditions to make the brittleness evaluations of different lithologies comparable; at the same time, the NDBC value range is limited to [0,1], which can effectively distinguish progressive failure from sudden failure with clear engineering significance.

In terms of crack evolution analysis, moment tensor analysis requires at least six sensors and specific layout conditions to determine the location, type (shear, tensile, composite) and event intensity of cracks, but it is limited by complex implementation conditions [12–14] and difficult to apply to engineering measurements; AF-RA analysis only needs one or two sensors on the sample surface and can distinguish crack types such as shear and tensile through simple analysis of AE event characteristic parameters, but the traditional AF-RA method requires manual setting of thresholds (AF/RA = 1~200), which has the problem of subjectivity [15]. Hu [16] used AF/RA = 70 as the dividing line

based on experiments. It is worth noting that Chen [17] and Huang [18] introduced the Gaussian mixture model (GMM) into the research of AE crack classification but did not evaluate the clustering results, nor did they conduct in-depth research on the impact of GMM structure on clustering results. Therefore, this paper discusses in detail the impact of data structure and model structure on clustering results and uses multiple indicators to evaluate the accuracy of GMM clustering results.

Taking an ultra-large underground mine as the engineering background, this study carried out AE monitoring on four main rock types (granite, phyllite, diabase and siliceous limestone) by the Brazilian splitting test method and analyzed the rock crack evolution process using the normalized damage–stress brittleness coefficient and AF-RA based on GMM clustering, providing theoretical support for the differentiated monitoring and prevention and control system of safe mining in mines.

2. Materials and Methods

2.1. Experimental Scheme

2.1.1. Sample Preparation

Static tensile tests of rocks mainly include two methods: direct tension and indirect tension (Brazilian splitting test). Although the tensile strength measured by the indirect tension is often overestimated, the Brazilian splitting test has become the main method due to its simple sample preparation and convenient operation [19]. The Brazilian splitting test has different loading methods: ISRM [20] recommends arc fixture contact, ASTM [21] recommends flat plate contact with samples, but the calculation formula for tensile strength is the same; Wang [22] proposed the flattened Brazilian disc test method with flat ends, which applies uniform load on the sample and can measure tensile strength, elastic modulus and fracture toughness simultaneously; Yu [23] analyzed the influence of load distribution form on the results of the Brazilian splitting test and gave the analytical solutions of the full-field displacement and stress of the disc in the ISRM test method. In this paper, the Brazilian splitting test method recommended by ISRM is adopted. Rock cores of four types (granite, phyllite, diabase and siliceous limestone) are sampled to make standard samples with Φ50 mm × 25 mm, and the test for each lithology should be repeated at least three times optimally. These four rock types tested in this study are the main lithologies encountered in this underground mine where the field monitoring work is carried out. They are widely distributed in the mining area and are closely related to the engineering stability of underground openings, making the results directly applicable to the geomechanical conditions of the project.

Meanwhile, basic physical parameters of rocks are measured using a balance, caliper, wave velocity meter and uniaxial compression test, and the basic parameters of selected rocks are shown in Table 1.

Table 1. Parameters of rock samples.

Lithology	ρ/g·cm^{-3}	V_p/m·s^{-1}	σ_c/MPa	E/GPa	ν
Granite	2.75	4347.83	105.34	58.32	0.20
Phyllite	2.71	4761.91	105.5	90.62	0.24
Diabase	3.09	4651.16	78.98	58.17	0.24
Siliceous limestone	3.08	4545.45	109.97	80.15	0.17

2.1.2. AE Monitoring Method and Test Process

The AE signal acquisition system adopted the PCI-express 8 acquisition card produced by Mistras Group, Inc. (Princeton Junction, NJ, USA). Four Nano30 sensors (also from Mistras Group, Inc.) were attached to the front and back surfaces of each sample using a

coupling agent, respectively. The sensors were connected to a preamplifier with a gain of 40 dB, a trigger threshold of 45 dB, and a sampling frequency of 10 MHz. The parameter settings adopted in this work have been widely used in existing rock fracture monitoring research, which can effectively capture microcrack acoustic emission signals and meet the test requirements [6,13,17]. The test acquisition system is shown in Figure 1. The loading system was a TAW-2000 servo-hydraulic testing machine equipped with Brazilian splitting fixtures (manufactured by Changchun New Testing Machine Co., Ltd. in Changchun, China), and the test was carried out according to the following steps:

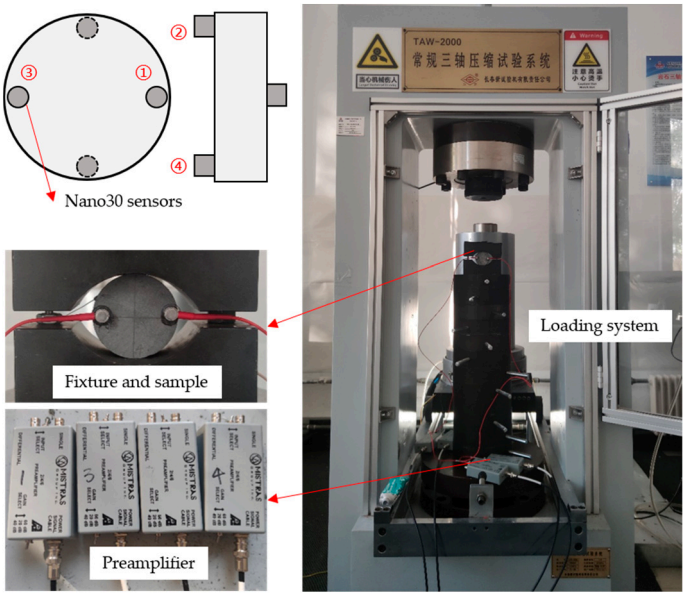


Figure 1. Test system.

(1) After the sample was installed, adjust the loading head of the testing machine to make the preload reach 1 kN; (2) attach AE sensors with glue and perform pencil lead break tests to confirm that each sensor can receive signals normally; (3) apply static loading at a rate of 0.1 mm/min (strain rate: 3.3×10^{-5} s^{-1}) and synchronously start the AE acquisition system until sample failure; (4) stop loading, shut down the AE system, and save the data.

2.2. Rock Brittleness Evaluation Based on AE

2.2.1. Correlation Between Lithology and AE Count, Peak Frequency Characteristics

Basic characteristic parameters of AE (e.g., count, energy, peak frequency, amplitude) can be used to analyze changes in the intrinsic properties of samples during the test. The ring count represents the number of oscillations of an AE signal when it exceeds the threshold per unit time; this indicator is highly sensitive to rock deformation and structural degradation and is therefore often used to demonstrate cumulative damage during the failure process. In the test, a higher ring count indicates greater internal damage to the rock [24], and a sudden increase in ring count can be regarded as a precursor to failure [25,26].

The peak frequency can be approximately regarded as the peak frequency of the AE signal, with a higher peak frequency indicating a smaller event source. The sampling frequency was set to 10 MHz, and the peak frequency was divided into three frequency bands: low frequency (0~128 kHz), medium frequency (125~256 kHz), and high frequency (256~500 kHz) [27], denoted as L, M, and H respectively. In compaction stage I (0~40%σ_t), low-frequency hits indicate the closure of microcracks or joint surfaces inside the rock and sliding of the sample during compression. In elastic stage II (40%~90%σ_t) and failure

stage III (>90%σ_t), low-frequency hits indicate the formation of new large-scale microcracks inside the sample, while medium- and high-frequency hits indicate the generation and propagation of small-scale cracks [28].

2.2.2. Normalized Damage–Stress Brittleness Coefficient

Brittleness reflects the mechanical behavior transition characteristic of rock from "stable bearing" to "sudden instability" and is a core indicator for measuring its failure mode (sudden or progressive). Common brittleness indices include B_1, B_2, B_3 [8], based on elastic modulus and Poisson's ratio, and B_4, B_5 [9] based on strength. In general, elastic indices (B_1–B_3) focus on the brittleness of materials in the small deformation stage (e.g., behavior before microcrack initiation), while strength indices (B_4, B_5) are suitable for evaluating the brittleness of materials in the final failure stage (e.g., differences in compressive and tensile strength at fracture). The calculation methods for indices B_1–B_5 are as follows:

$$B_1 = 0.5(E_{BRIT} + v_{BRIT}) \tag{1}$$

$$B_2 = \frac{E}{v} \tag{2}$$

$$B_3 = \frac{E_{BRIT}}{v_{BRIT}}, E_{BRIT} = \frac{E - E_{\min}}{E_{\max} - E_{\min}}, v_{BRIT} = \frac{v - v_{\min}}{v_{\max} - v_{\min}} \tag{3}$$

$$B_4 = \frac{\sigma_c}{\sigma_t} \tag{4}$$

$$B_5 = \frac{\sigma_c - \sigma_t}{\sigma_c + \sigma_t} \tag{5}$$

where E_{BRIT} and ν_{BRIT} are the normalized elastic modulus and normalized Poisson's ratio, respectively; E, $E_{\max}$ and $E_{\min}$ are the average, maximum, and minimum values of elastic modulus; v, $v_{\max}$ and $v_{\min}$ are the average, maximum, and minimum values of Poisson's ratio; σ_c and σ_t are the compressive strength and tensile strength, respectively. For B_1–B_3, a larger elastic modulus and smaller Poisson's ratio indicate stronger brittleness. For B_4 and B_5, high resistance to compression but low resistance to tension indicates strong brittleness.

Elastic indices only consider parameters such as elastic modulus and Poisson's ratio and cannot reflect inelastic behaviors such as plastic deformation and microcrack propagation that rocks may undergo before failure, which may lead to misjudgment by elastic indices. In addition, indices B_1 and B_3 rely on the normalization of E_{BRIT} and ν_{BRIT}, and the reliability of their results is greatly affected by the subjectivity in selecting extreme values; B_2 directly uses the ratio of original parameters and is thus susceptible to dimensionality and absolute values.

Although strength-based indices evaluate brittleness from the perspective of failure characteristics, they also face numerous challenges. Rocks exhibit significant resistance to compression but vulnerability to tension, and measurement errors in tensile strength σ_t can significantly affect the accuracy of B_4 and B_5. These indices only consider the compressive–tensile strength ratio under uniaxial stress conditions, ignoring the prevalent compression–shear composite stress states in actual engineering, which may underestimate the risk of sudden failure in high-brittleness rocks. For layered rocks with obvious anisotropic characteristics (e.g., shale and schist), strength indices also fail to reflect brittleness differences in different directions.

The normalized damage–stress brittleness coefficient (NDBC, denoted as B_6) is proposed to characterize the brittleness of rock during the damage–fracture process, which is defined as the normalized integral of the acoustic emission (AE) cumulative count over the entire stress–time process, reflecting the correlation between AE activity and rock brittle failure.

(1) Stress normalization

To eliminate the difference in peak strength among different rock types, the real-time stress is uniformly normalized:

$$\sigma^* = \frac{\sigma}{\sigma_t} \tag{6}$$

where σ is real-time stress, σ_t is tensile strength, σ^* is normalized stress (range [0,1]).

(2) Damage variable

During loading, AE activity directly reflects the internal microcrack initiation, propagation and cumulative damage of rock specimens. Therefore, the damage variable D is defined as the ratio of cumulative AE count at any moment to the total AE count throughout the entire loading process (from initial loading to final failure) [11]:

$$D = \frac{N_t}{N_{total}} \tag{7}$$

where N_t is the cumulative AE count at a certain loading moment and N_{total} represents the total cumulative AE count at the failure stage.

The damage variable D is normalized within the range [0,1], which realizes the unified quantitative characterization of rock internal damage.

(3) Calculating NDBC

Combined with normalized stress, a standardized damage–stress evolution curve is established.

The area enclosed by the damage–stress curve and the horizontal axis is defined as the novel brittleness index B_6 (NDBC).

$$B_6 = \int D d_{\sigma^*} \tag{8}$$

For high-brittleness rock, microcrack development and AE activities are restrained in the compaction and elastic stages, and internal damage accumulates slowly.

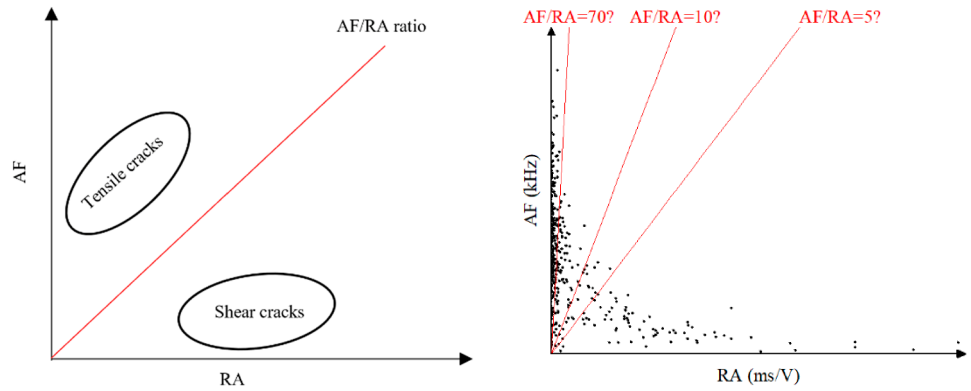
Sharp damage acceleration and rapid microcrack coalescence only occur near the peak stress, resulting in a smaller enclosed area of the stress–damage curve.

Consequently, the smaller the B_6 value, the stronger the rock brittleness, which can effectively distinguish the brittle differences of different lithologies.

2.3. Rock Crack Evolution Mechanism Based on GMM

2.3.1. AF-RA Analysis

The surrounding rock crack evolution model serves as a bridge connecting microdamage and macrodisasters, acting both as a decoder for explaining disaster causes and a navigation map for achieving controllable risks. AF-RA analysis is a classic method for crack classification. The RA value is the ratio of rise time to maximum amplitude in a single AE signal, and the AF value is the ratio of ring count to duration. A high AF and low RA indicate tensile cracks and vice versa for shear cracks. The basic principle of AF-RA analysis is shown in Figure 2a: bounded by the AF/RA ratio line, the left region corresponds to tensile cracks, and the right region represents shear cracks. However, a key limitation of this method is that crack classification results are highly dependent on the slope setting of the AF/RA dividing line. As shown in Figure 2b, traditional methods adopt an artificially preset slope range (1~200) [15], but different slope selections can lead to significant classification differences [29,30], which seriously affects the objectivity of analysis results.



(**a**) (**b**)

Figure 2. The AF-RA crack classification method: (**a**) the classification principle, (**b**) the results depend on the AF/RA ratio.

2.3.2. Crack Classification Based on GMM

To address this issue, this study introduces the Gaussian mixed model (GMM). As a probabilistic model based on the linear combination of multiple Gaussian distributions, a GMM can effectively identify potential multiple distribution patterns in datasets. Compared with hard clustering methods such as K-means, a GMM can more accurately describe complex data distribution characteristics through probabilistic modeling, while significantly reducing subjective deviations caused by artificially setting classification boundaries.

The density distribution function of the GMM is expressed as:

$$p(x_i) = \sum_{k=1}^{K} \omega_k p_k(x) = \sum_{k=1}^{K} \omega_k N(x|u_k, \Sigma_k) \tag{9}$$

where K is the number of Gaussian components, ω_k is the weight of each component, $N(x|\mu_k,\Sigma_k)$ is the probability density function of the k-th Gaussian distribution, $x = \{x_1, x_2, \ldots, x_n\}$ represents the sample, μ_k is the $K \times 1$ mean vector, Σ_k is the $k \times k$ covariance matrix.

$$N(x|\mu_k, \sum_k) = \frac{e^{-\frac{1}{2}(x-\mu_k)^{\mathrm{Trans}}\sum_k{}^{-1}(x-\mu_k)}}{2\pi^{n/2}|\sum_k|^{1/2}} \tag{10}$$

Among them, Gaussian components can use the same covariance matrix Σ_k (i.e., a shared covariance matrix). The advantages of a shared covariance matrix include stable calculation results (especially strong stability with small samples) and high computational efficiency; for two Gaussian components with a shared covariance matrix, the decision boundary is usually a straight line. If each Gaussian component uses an unshared covariance matrix, the computational complexity increases and the calculation stability is poor with small samples; however, when each cluster has a different shape or direction, an unshared covariance matrix can achieve a better fitting effect, and the decision boundary is usually a curve.

Considering the failure characteristics of the Brazilian splitting experiment, rock damage is dominated by two typical crack forms: tensile crack and shear crack. From the perspective of physical mechanism and fracture mode, the actual crack types are limited to two categories. Thus, the number of GMM components was set to 2, avoiding subjective artificial selection of cluster numbers and ensuring classification results conform to the intrinsic fracture mechanism of rock. For the algorithm solution, the EM iterative stopping threshold was set to 10^{-6} to ensure stable convergence. To evaluate the sensitivity of the GMM to random initialization, the clustering operation was repeated 10 times

independently with identical input features and a fixed cluster number of 2. No obvious category reversal or abnormal classification occurred.

Evaluation indicators for clustering results include the Silhouette coefficient, Calinski–Harabasz (CH) index, Davies–Bouldin (DB) index, etc.

$$Silhouette = \frac{b(i) - a(i)}{\max(a(i), b(i))} \tag{11}$$

$$DB = \frac{1}{k}\sum_{i=1}^{k} \max_{j \neq i}\left(\frac{d_i + d_j}{D(c_i, c_j)}\right) \tag{12}$$

$$CH = \frac{B(k)/(k-1)}{W(k)/(n-k)} \tag{13}$$

The Silhouette coefficient reflects the similarity of a sample to other samples in its own cluster compared to its similarity to samples in other clusters, with a value range of $[-1, 1]$; a larger value indicates better clustering performance. Herein, $a(i)$ is the average distance from sample i to all other samples in the same cluster, and b(i) is the average distance from sample i to all samples in the nearest other cluster (excluding its own cluster).

The Davies–Bouldin (DB) index is a method for evaluating clustering performance based on the ratio of inter-cluster separation to intra-cluster compactness; a smaller value indicates better clustering performance, with an ideal value close to 0. Herein, k is the number of clusters; $d(i)$ is the average distance from all samples in cluster i to the cluster center; D(c_i,c_j) is the Euclidean distance between the centers of cluster i and cluster j.

The Calinski–Harabasz (CH) index measures clustering validity by comparing inter-cluster dispersion and intra-cluster dispersion; a larger value indicates greater differences between clusters and higher compactness within clusters. Herein, $B(k)$ is the inter-cluster dispersion (i.e., the total sum of squares between all cluster centers and the global center); $W(k)$ is the intra-cluster dispersion (i.e., the sum of squares of distances from all samples to their respective cluster centers).

Taking siliceous limestone as an example, the original data, globally standardized data, and clustering results under shared and unshared covariance matrices are shown in Table 2.

Table 2. Evaluation of clustering results for data structures and model structures.

	Silhouette ↑		**DB ↓**		**CH ↑**	
	Original Data	**Standardized Data**	**Original Data**	**Standardized Data**	**Original Data**	**Standardized Data**
Shared covariance matrices	0.4690	0.8682	0.8595	0.7153	96.0	367.2
Unshared covariance matrices	0.3470	0.5903	1.4997	1.4690	213.6	295.9

The indicators show that GMM clustering is sensitive to data structure. Compared with the original AF and RA data, all indicators are significantly improved after global standardization, with the CH index increasing by up to 2.8 times; the model using a shared covariance matrix also outperforms the model with an unshared covariance matrix across all indicators. Therefore, this study adopts the GMM with a shared covariance matrix and global standardized data.

3. Results

3.1. Tensile Strength

For Brazilian splitting tests, the tensile strength is calculated according to the following formula:

$$\sigma_t = \frac{2P}{\pi dt} \tag{14}$$

where σ_t is the tensile strength, MPa; P is the peak load, N; d is the diameter, mm; t is the thickness, mm.

The experiment involved four types of rock lithologies, and the true sample size for each lithology is as follows: granite (n = 3), phyllite (n = 4), diabase (n = 3), and siliceous limestone (n = 3). All specimens were prepared in strict accordance with the relevant standards, and all valid test data are reported to ensure the authenticity and comprehensiveness of the experimental results. The tensile strength of the rocks is shown in Table 3.

Table 3. Tensile strength.

Lithology	Sample Size/n	σ_t/MPa	Tensile Strength (Mean ± SD)/MPa
Granite	3	14.87, 16.44, 16.09	15.80 ± 0.83
Phyllite	4	14.38, 12.47, 12.93, 15.30	13.77 ± 1.30
Diabase	3	15.50, 14.54, 16.33	15.46 ± 0.89
Siliceous limestone	3	6.77, 7.87, 7.24	7.29 ± 0.55

One-way analysis of variance (one-way ANOVA) was performed to find the significance of tensile strength differences among the four lithologies. The results show that F = 48.88, $p = 6.79 \times 10^{-6} < 0.001$, indicating extremely significant differences in tensile strength between different rock types. Combined with the mean and standard deviation, the data dispersion within each group is low, confirming the reliability of the experimental results.

3.2. Lithology and Peak Frequency Characteristics

The peak frequency distribution during the tests of several rocks is shown in Figure 3, and the proportion of AE peak frequencies in each stage is presented in Table 4.

(1) In the compaction stage I, AE hits are limited and sporadic, accounting for approximately 5% of the total, and are dominated by medium- and high-frequency hits. This indicates that AE in this stage is mainly caused by the closure of primary cracks and small-scale failures such as sample torsion.

(2) In the elastic stage II, AE activity of granite is prominent, accounting for 63.2% of the total hits, all of which are medium- and high-frequency hits, indicating that its failure process is characterized by continuous small-scale cracks. The other three types of rocks exhibit less AE activity, with proportions ranging from 10% to 20%, indicating that their failure is not obvious in this stage.

(3) In the failure stage III, except for granite, the failure is concentrated in this stage. Phyllite experiences frequent low-frequency hits, indicating the generation of a large number of new large-scale cracks inside and their rapid propagation. Siliceous limestone has the highest proportion of new cracks (81%), but the total number of AE hits remains low, indicating that internal failure is not obvious, and most energy is stored and released intensively at the moment of failure, resulting in sudden instability, which manifests as overall fragmentation and disintegration in engineering practice. Diabase has the highest total number of AE hits, with numerous high- and low-frequency hits, indicating diverse and continuous internal failure modes.

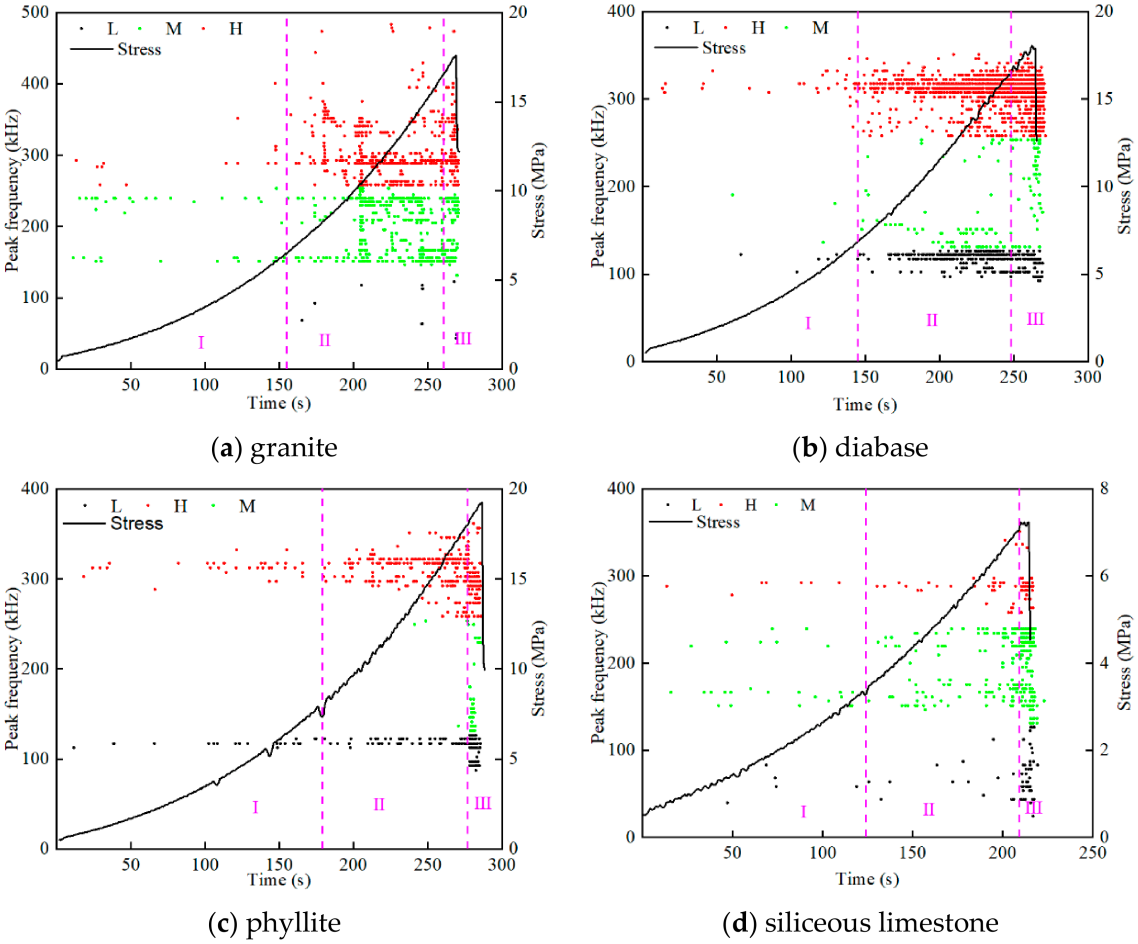


Figure 3. Stress and peak frequency characters of rocks (pink dashed lines divide loading stages).

Table 4. Distribution of peak frequency.

Lithology	Total Hits	Compaction Stage			Elastic Stage			Failure Stage		
		L	M	H	L	M	H	L	M	H
Granite	2132	0	1.9%	0.7%	0.7%	31.1%	31.4%	0.1%	16.6%	17.5%
Phyllite	1100	1.8%	0.0%	3.1%	2.8%	0.2%	12.0%	36.1%	4.5%	39.5%
Diabase	3173	0.3%	0.3%	2.1%	5.5%	1.4%	14.1%	9.9%	3.0%	63.4%
Siliceous limestone	578	1.0%	4.6%	1.4%	1.2%	9.1%	1.7%	10.9%	54.7%	15.4%

3.3. Brittleness and AE Count Characteristics

The numbers of AE counts and cumulative counts in each stage are shown in Table 5. The relationships between AE count, cumulative count and stress during the tests of the four rock samples are presented in Figure 4.

Table 5. Count and accumulated counts in each phase.

Lithology	Compaction Stage		Elastic Stage		Failure Stage	
	Count	Accumulated Count	Count	Accumulated Count	Count	Accumulated Count
Granite	56	3728	1352	148,868	724	95,067
Phyllite	54	1934	165	7543	881	67,635
Diabase	87	2599	663	45,317	2423	177,404
Siliceous limestone	40	1161	70	4261	474	65,590

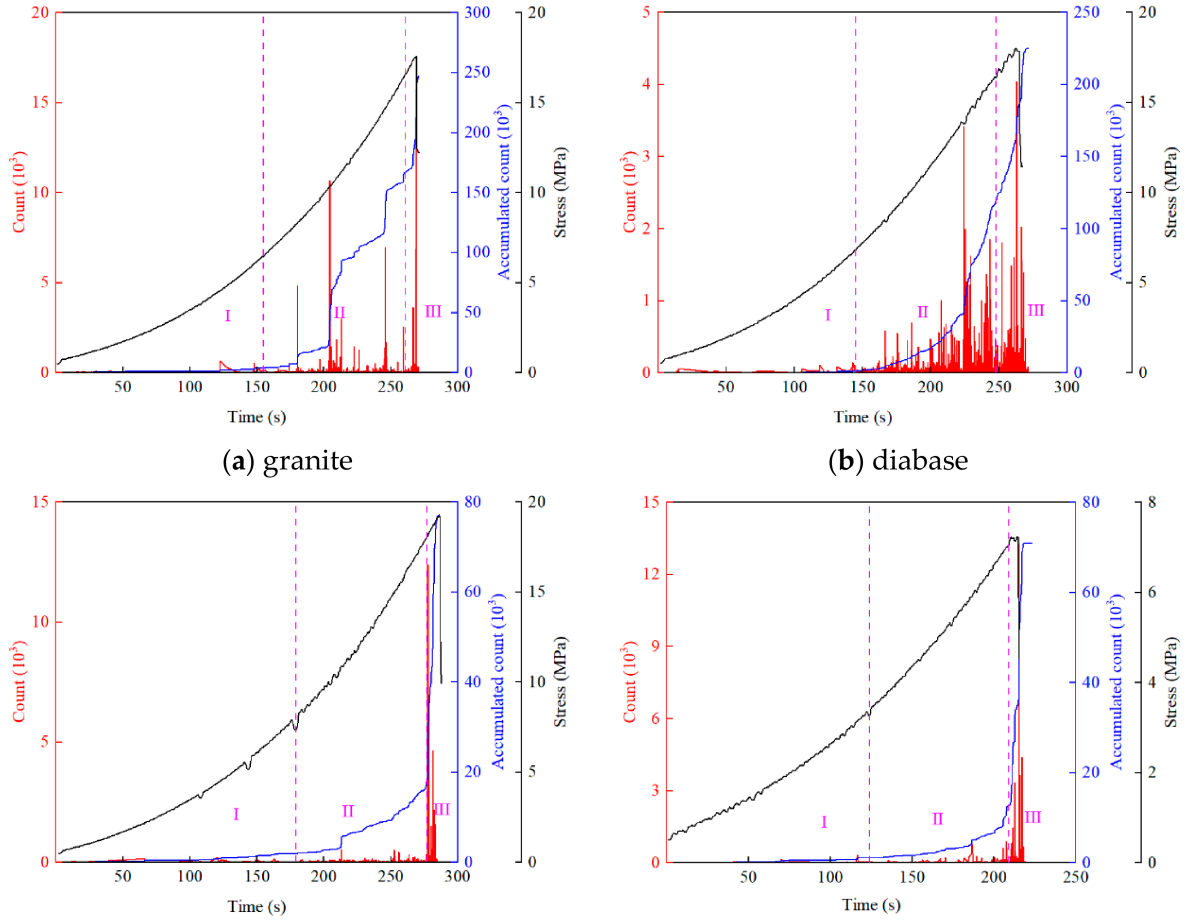


Figure 4. Count and accumulated count with stress (pink dashed lines divide loading stages).

As can be seen from Table 5 and Figure 4, count directly reflects the activity of acoustic emission. Diabase exhibits the highest number of counts, with the proportions of hits in the elastic stage and failure stage being 20.89% and 76.36%, respectively, indicating that the formation and development of microcracks inside diabase accompany the entire loading process. Granite shows a similar trend to diabase but differs in that the proportions of hits in the elastic stage and failure stage are 63.06% and 34.28%, respectively, suggesting that granite sustains greater damage in the elastic stage. Phyllite and siliceous limestone have a lower number of hits, which are mainly concentrated in the failure stage (80.1% for phyllite and 81.02% for siliceous limestone), with their cumulative count proportions reaching 87.71% and 92.36%, respectively. This indicates that AE activity is inactive in the first two stages, and internal microcrack development is limited, reflecting that they possess higher brittleness compared to diabase and granite. Meanwhile, the AE hits with the highest counts all occur in stage III (17,461 hits for granite at 94.7% σ_t, 12,398 hits for phyllite at 94.59% σ_t, 4043 hits for diabase at 95.62% σ_t, and 13,248 hits for siliceous limestone at 96.19% σ_t), indicating that internal microcracks interconnect at this point, and the material will immediately lose load-bearing capacity and undergo macroscopic failure.

Due to the varying durations of each test, stress normalization was performed to facilitate comparative analysis and to evaluate brittleness using B_6. The damage curves of each sample are shown in Figure 5.

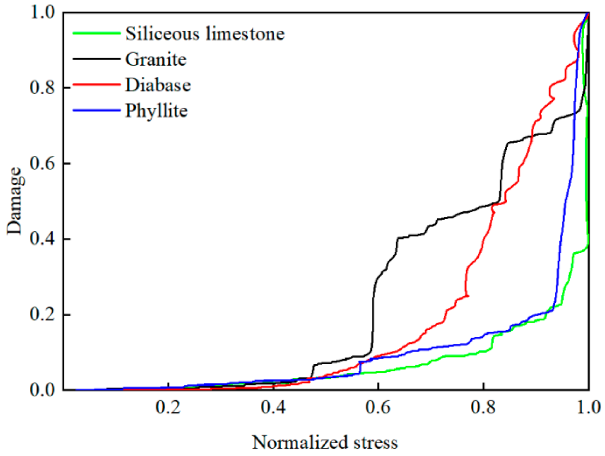


Figure 5. The normalized damage–stress curves of the rocks.

As can be seen from the curves, the damage curves of siliceous limestone and phyllite are similar, showing a sharp increase before failure, which reflects strong brittleness. The damage of granite and diabase accumulates gradually until failure. The evaluation of the four rock types using various brittleness indices is presented in Table 6.

Table 6. Brittleness index of rocks.

Brittleness Index	Granite	Phyllite	Diabase	Siliceous Limestone
B_1	0.39	0.42	0.49	0.54
B_2	296.53	382.92	245.79	483.06
B_3	1.37	1.04	0.85	0.94
B_4	6.67	6.83	5.73	15.08
B_5	0.74	0.74	0.70	0.88
B_6	0.23	0.10	0.18	0.07

Pearson correlation coefficients between the proposed NDBC (B_6) and five traditional brittleness indices (B_1–B_5) were calculated, as listed in Table 7. The Pearson correlation results show that NDBC (B_6) exhibits consistent trends with traditional brittleness indices B_1, B_2, B_4 and B_5 (higher B_1, B_2, B_4, B_5 and lower B_6 indicate strong brittleness). In contrast, B_3 shows negative correlations with these conventional indices and a positive correlation with B_6. This indicates that the brittleness ranking given by B_3 is inconsistent with the majority of widely accepted brittleness indices, suggesting potential limitations in the applicability of B_3 under the test conditions of this study. Compared with B_3, the proposed NDBC is more consistent with the mainstream brittleness evaluation framework, which further confirms its rationality.

Table 7. Pearson correlation analysis.

	B_1	B_2	B_3	B_4	B_5	B_6
B_1	1.00					
B_2	0.47	1.00				
B_3	−0.80	−0.16	1.00			
B_4	0.72	0.89	−0.25	1.00		
B_5	0.62	0.92	−0.14	0.99	1.00	
B_6	−0.61	−0.86	0.58	−0.70	−0.69	1.00

To evaluate the robustness of the proposed NDBC (B_6) against common experimental fluctuations in acoustic emission data, sensitivity analysis was conducted by introducing

±5% and ±10% random noise to AE count. The perturbed data were reaccumulated to maintain the normalization of the damage variable D.

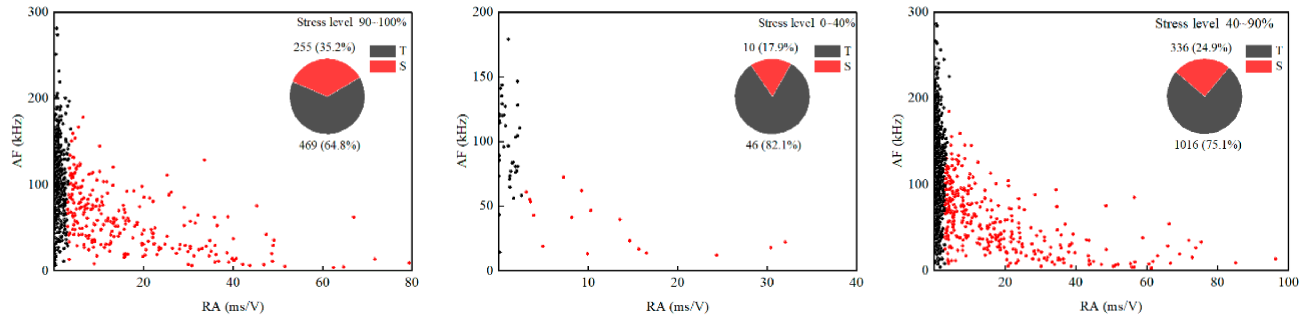
The results, presented in Table 8, show that the relative error of NDBC remains below 7.2% under both ±5% and ±10% noise perturbations. Notably, the brittleness ranking of the four rock types remains consistent with the original results, indicating that NDBC exhibits good stability and low parameter sensitivity. Its brittleness evaluation is robust to minor measurement errors and data fluctuations in acoustic emission monitoring.

Table 8. Sensitivity analysis of NDBC under ±5% and ±10% noise perturbations in AE count.

	Granite	Phyllite	Diabase	Siliceous Limestone
B_6 (Original)	0.234480	0.100443	0.184953	0.074611
B_6 (±5% noise)	0.234249	0.100552	0.173446	0.079949
Relative error	0.10%	0.11%	6.22%	7.16%
B_6 (±10% noise)	0.235319	0.101325	0.174066	0.079931
Relative error	0.36%	0.88%	5.89%	7.13%

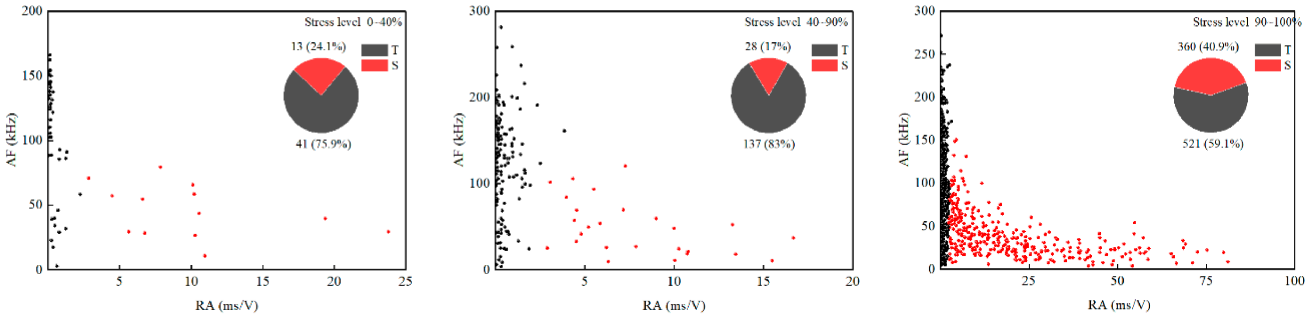
3.4. Crack Evolution and Failure Types During Failure Process

As mentioned earlier, this study adopts the GMM with a shared covariance matrix and standardized AF-RA data to conduct cluster analysis on cracks of AE hits in each stage of the Brazilian splitting tests for the four rock types. The crack types are statistically analyzed in three stages: 0~40%σ_t, 40%~90%σ_t, and 90%~100%σ_t, as shown in Figures 6–9, where T (black dots) represents tensile cracks and S (red dots) represents shear cracks.



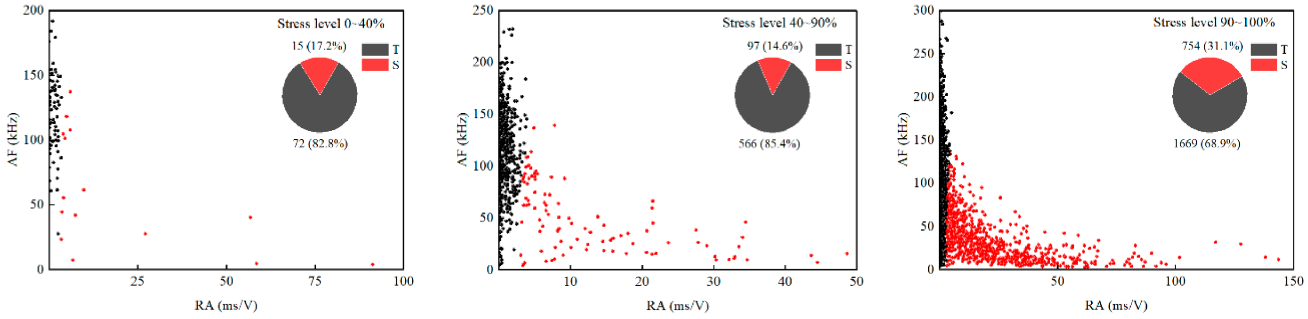
(**a**) 0~40%σ_t (**b**) 40%~90%σ_t (**c**) 90%~100%σ_t

Figure 6. The crack clustering of granite Brazilian test.



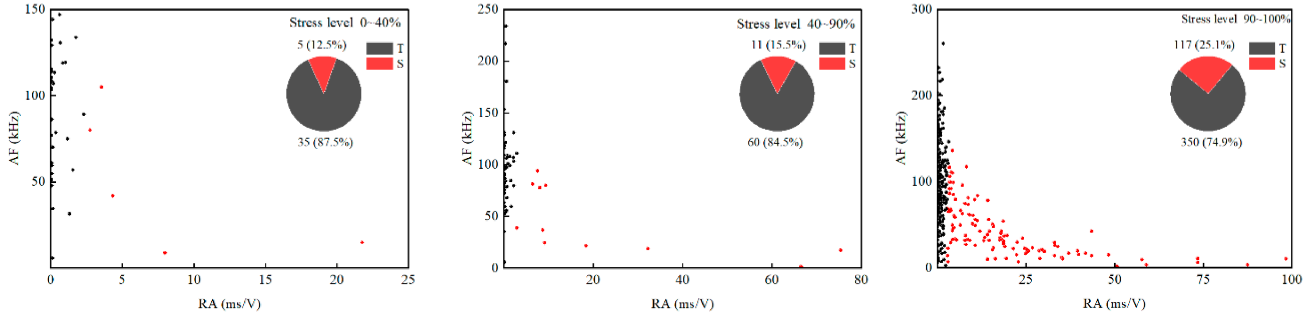
(**a**) 0~40%σ_t (**b**) 40%~90%σ_t (**c**) 90%~100%σ_t

Figure 7. The crack clustering of phyllite Brazilian test.



(**a**) 0~40%σ_t (**b**) 40%~90%σ_t (**c**) 90%~100%σ_t

Figure 8. The crack clustering of diabase Brazilian test.



(**a**) 0~40%σ_t (**b**) 40%~90%σ_t (**c**) 90%~100%σ_t

Figure 9. The crack clustering of siliceous limestone Brazilian test.

As can be seen from Figures 6–9, the total proportion of tensile cracks throughout the entire process is 71.81% for granite, 63.55% for phyllite, 72.71% for diabase, and 76.99% for siliceous limestone.

(1) Despite differences in lithology, the proportion of tensile cracks remains high (75.1%~87.5%) during the compaction and elastic stages, indicating that internal rock cracks are dominated by tensile cracks at low stress levels.

(2) During the failure stage, the proportion of tensile cracks decreases while that of shear cracks increases. This process can be referenced to the tensile earthquake model, as shown in Figure 10: Σ denotes the seismic plane, $\boldsymbol{n}$ its normal vector, [$\boldsymbol{u}$] the slip vector, and α the dip angle of the slip vector ($\alpha = 0°$ for pure shear earthquakes and $\alpha = 90°$ for pure tensile earthquakes). This indicates that, under splitting load, failure at low stress levels is mainly characterized by the opening between two crack surfaces; near failure, the opening of crack surfaces leads to a decrease in their load-bearing capacity, and dislocation along the crack surfaces exacerbates rock instability.

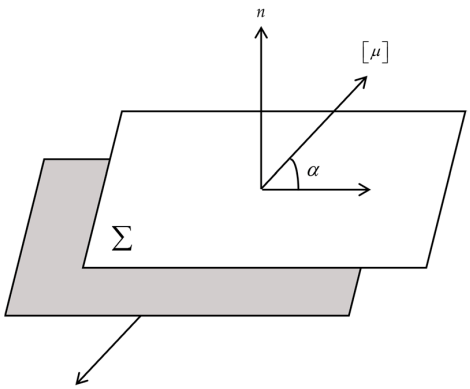


Figure 10. The tensile earthquake model [31].

To further verify the rationality of the crack classification results obtained by GMM clustering, the macroscopic fracture morphology of typical granite specimens under the Brazilian splitting test was analyzed.

As shown in Figure 11, the granite specimen presents a central splitting failure mode under diametral loading, with the main crack propagating along the loading axis from the center to the edge of the disk. This typical straight splitting crack is the most representative tensile fracture morphology in the Brazilian test, characterized by a smooth, flat fracture plane without obvious friction or sliding traces.



Figure 11. Macroscopic tensile splitting crack of granite specimen under Brazilian test. The main crack confirms the tensile-dominated failure mode, which is consistent with the GMM-based crack classification results.

The GMM clustering results show that tensile cracks dominate in granite specimens, which is highly consistent with the observed macroscopic splitting failure mode. This direct visual evidence confirms the reliability of the AE signal classification and crack identification in this study.

4. Discussion

As described in Section 2.3, the AF-RA ratio k directly affects the classification of acoustic emission crack types. The selection of k is discussed in combination with the GMM algorithm. It should be emphasized that the GMM algorithm is used here as an unsupervised clustering tool for preliminary classification of AE signals, and the crack-type classification results from GMM are cross-validated with the inherent tensile-dominated failure characteristics of the Brazilian test and the observed macroscopic splitting fracture morphology (Section 3.4 and Figure 11). The overall agreement supports that the GMM classification is a reasonable reference for calibration.

The literature [15] recommends a k value ranging from 1 to 200. It is found that, when k is excessively large, the AF-RA dividing line approaches the y-axis, causing points clustered near the y-axis to be identified as shear cracks, as shown in Figure 12a. When k = 30, the results are close to those of the GMM. As k continues to increase, some tensile cracks are misclassified as shear cracks. Furthermore, k is divided into 10 groups. Each AF-RA point is classified, and the results are compared with those of the GMM. The consistency rate is shown in Figure 12b. As k increases from 10 to 20~30, the consistency of crack type classification between the two methods reaches its maximum. With a further increase in k, the AF-RA dividing line moves closer to the y-axis, leading to deviations in the classification

of some cracks. Different lithologies cause certain differences in the crack classification results of the two methods, but satisfactory results can be achieved when k = 20~30.

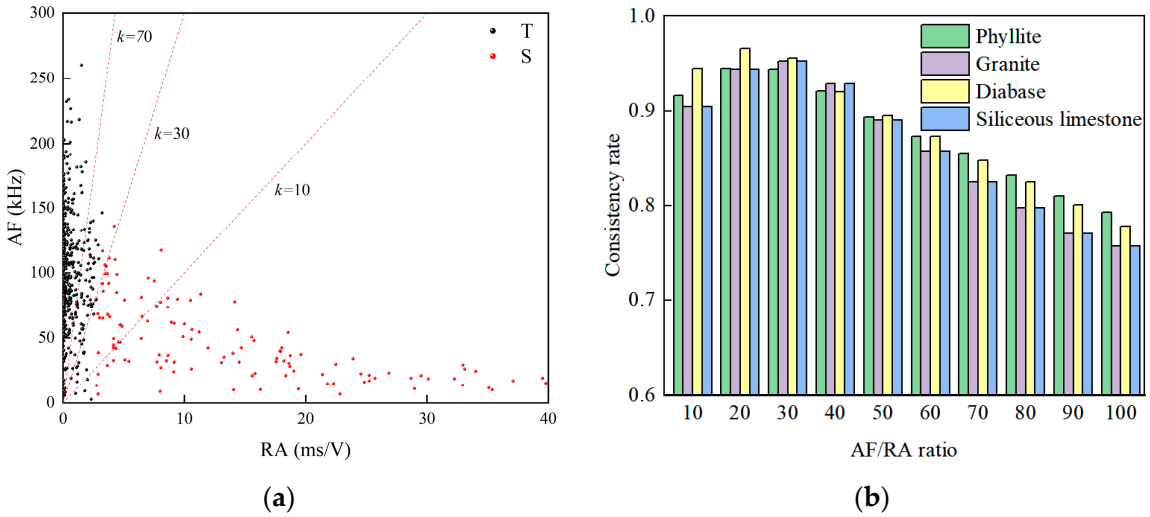


Figure 12. The classification of cracks by different AF/RA ratios. (**a**) k determines a tensile or shear crack; (**b**) consistency of crack classification between traditional method and GMM method under different k values.

It should be noted that this study only conducted tests on four main lithologies of this underground mine. Future work will include more rock types and engineering cases (e.g., different confining pressures, loading rates) to further verify the generalization ability of the proposed method.

5. Conclusions

(1) The dominant frequency characteristics of acoustic emission (AE) reflect the failure mode of rocks under splitting load. High brittleness and dense rocks (e.g., siliceous limestone) are characterized by medium- and high-frequency AE hits near the moment of failure, exhibiting sudden instability. Weakly brittle rocks (e.g., granite) undergo gradual damage accumulation until instability under load, with no obvious failure precursors.

(2) Rock damage was defined based on cumulative AE counts during the splitting process, and a rock brittleness index was established according to normalized damage–stress. The results show that siliceous limestone has the highest brittleness index (0.07), while granite has the lowest (0.23), which is in good agreement with the results of several commonly used brittleness indices.

(3) The Gaussian mixed model (GMM) algorithm can effectively analyze the crack evolution law during splitting. Tensile cracks dominate throughout the loading process: the proportion of tensile cracks reaches 75.1%~87.5% when the stress level is below 90%σ_t and decreases to 60%~75% near failure. After tensile cracks open to a certain extent, dislocation occurs along the crack surfaces; as stress increases, rock failure transitions from tensile-dominated to a combination of tension and shear.

(4) The roof and floor of the orebody in this underground mine are mainly composed of granite and phyllite, with local siliceous limestone. Due to its high brittleness and sudden failure characteristics, siliceous limestone faces greater instability risks and potential threats of overall collapse during mining. Therefore, real-time monitoring should be strengthened and targeted prevention and control measures adopted in areas containing siliceous limestone to ensure the safety and stability of mining operations.

Author Contributions: Conceptualization, X.C.; methodology, C.C.; software, X.C.; validation, C.C.; resources, L.B.; data curation, L.B.; writing—original draft preparation, X.C.; writing—review and editing, C.W.; funding acquisition, C.W. All authors have read and agreed to the published version of the manuscript.

Funding: This research was funded by National Key Research and Development Program of China, grant number 2024YFC2909500.

Data Availability Statement: The data presented in this study are available on request from the corresponding author. The data are not publicly available due to privacy or ethical restrictions.

Acknowledgments: The authors gratefully acknowledge the technical support provided by Bo Pan during the experiment. During the preparation of this manuscript, the authors used artificial intelligence tools for language polishing and text optimization. The authors have reviewed and revised all content and take full responsibility for the published work.

Conflicts of Interest: Authors Chong Chen and Li Bi were employed by the company Ansteel Beijing Research Institute Co., Ltd. and Ansteel Cornerstone Mining Co., Ltd. The remaining authors declare that the research was conducted in the absence of any commercial or financial relationships that could be construed as a potential conflict of interest.

Abbreviations

The following abbreviations are used in this manuscript:

AE	Acoustic Emission
GMM	Gaussian Mixed Model
NDBC	Normalized Damage–Stress Brittleness Coefficient
AF	Average Frequency
RA	Risetime/Amplitude

References

1. Zhang, Y.; Su, S.; Yu, G.; Su, Y.; Li, J. Influential Factors of Stability of Silica Stone Cuesta Cutting Slope. *J. Yangtze River Sci. Inst.* **2018**, *35*, 121–126.
2. Golshani, A.; Okui, Y.; Oda, M.; Takemura, T. A micromechanical model for brittle failure of rock and its relation to crack growth observed in triaxial compression tests of granite. *Mech. Mater.* **2006**, *38*, 287–303. [CrossRef]
3. Li, X.; Huai, Z.; Li, X.B. Study on Fracture Characteristics and Mechanical Properties of Brittle Rock Based on Crack Propagation Model. *Gold Sci. Technol.* **2019**, *27*, 41–51.
4. Yao, Q.; Wang, W.; Yang, S.; Fang, J.; Zhou, B. Direct shear and acoustic emission characteristics of sandy mudstone under the effect of moisture content. *J. China Coal Soc.* **2021**, *46*, 2910–2922.
5. Fu, H.; Li, H.; Li, X. Research on the range of fracture process zone of granite based on DIC and acoustic emission. *Chin. J. Rock Mech. Eng.* **2022**, *41*, 2497–2508.
6. Khadivi, B.; Heidarpour, A.; Zhang, Q.; Masoumi, H. Characterizing the cracking process of various rock types under Brazilian loading based on coupled Acoustic Emission and high-speed imaging techniques. *Int. J. Rock Mech. Min. Sci.* **2023**, *168*, 105417. [CrossRef]
7. Guo, S.H. *Study on Crack Evolution and Mechanical Mechanism of Anchored Rock Mass*; China University of Mining Technology: Xuzhou, China, 2019.
8. Guo, Z.; Li, X.Y.; Liu, C.; Feng, X.; Shen, Y. A shale rock physics model for analysis of brittleness index mineralogy and porosity in the Barnett Shale. *J. Geophys. Eng.* **2013**, *10*, 25006–25015. [CrossRef]
9. Altindag, R. The correlation of specific energy with rock brittleness concept on rock cutting. *J. S. Afr. Inst. Min. Metall.* **2003**, *103*, 163–171.
10. Zhao, K.; Song, Y.; Yan, Y.; Gu, S.; Wang, J.; Guo, X.; Luo, C.; Suo, T. Mechanics and acoustic emission fractal characteristics of surrounding rock of tantalum–niobium mine under splitting condition. *Nat. Resour. Res.* **2022**, *31*, 149–162. [CrossRef]
11. Zhao, Y.X.; Sun, Z.; Liu, B. Comparative study of semi-circular bending tests for modes I and II fracture characteristics of Xinzhouyao bituminous coal. *Chin. J. Rock Mech. Eng.* **2019**, *38*, 1593–1604.
12. Eyre, T.S.; van der Baan, M. Overview of moment-tensor inversion of microseismic events. *Lead Edge* **2015**, *34*, 882–888. [CrossRef]
13. Sun, W.; Wu, S. A study of crack initiation and source mechanism in the Brazilian test based on moment tensor. *Eng. Fract. Mech.* **2021**, *246*, 107622. [CrossRef]

14. Ma, J.; Wu, S.; Zhang, X.-P.; Gan, Y. Modeling acoustic emission in the Brazilian test using moment tensor inversion. *Comput. Geotech.* **2022**, *123*, 103567. [CrossRef]
15. Ohno, K.; Ohtsu, M. Crack classification in concrete based on acoustic emission. *Constr. Build. Mater.* **2010**, *24*, 2339–2346. [CrossRef]
16. Hu, X.; Su, G.; Chen, G.; Mei, S.; Feng, X.; Mei, G.; Huang, X. Experiment on rockburst process of borehole and its acoustic emission characteristics. *Rock Mech. Rock Eng.* **2019**, *52*, 783–802. [CrossRef]
17. Chen, Z.; Zhang, G.; He, R.; Tian, Z.; Fu, C.; Jin, X. Acoustic emission analysis of crack type identification of corroded concrete columns under eccentric loading: A comparative analysis of RA-AF method and Gaussian mixture model. *Case Stud. Constr. Mater.* **2023**, *18*, e02021. [CrossRef]
18. Huang, X.; Dong, S.; Li, J.; Lu, Y. Research on granite crack identification by acoustic emission based on GMM+SVM. *Min. Saf. Environ. Prot.* **2022**, *49*, 21–28.
19. Wang, Y.S.; Deng, J.H.; Li, L.R.; Zhang, Z.H. Micro failure Analysis of Direct and Flat Loading Brazilian Tensile Tests. *Rock Mech. Rock Eng.* **2009**, *52*, 4175–4187. [CrossRef]
20. ISRM. Suggested methods for determining tensile strength of rock materials. *Int. J. Rock Mech. Min. Sci. Geomech. Abstr.* **1978**, *15*, 99. [CrossRef]
21. *ASTM D3967-16*; Standard Test Method for Splitting Tensile Strength of Intact Rock Core Specimens. ASTM International: West Conshohocken, PA, USA, 2016.
22. Wang, Q.Z.; Wu, L.Z. The flattened Brazilian disc specimen used for determining elastic modulus, tensile strength and fracture toughness of brittle rocks: Experimental results. *Int. J. Rock Mech. Min. Sci.* **2004**, *41*, 26–30. [CrossRef]
23. Yu, J.H.; Shang, X.C.; Wu, P.F. Influence of pressure distribution and friction on determining mechanical properties in the Brazilian test: Theory and experiment. *Int. J. Solids Struct.* **2019**, *161*, 11–22. [CrossRef]
24. Pan, J.; Wu, X.; Guo, Q.; Xi, X.; Cai, M. Uniaxial experimental study of the deformation behavior and energy evolution of conjugate jointed rock based on AE and DIC methods. *Adv. Civ. Eng.* **2020**, *2020*, 8850250. [CrossRef]
25. Guo, J.; Liang, S.; Zhang, H.; Sun, F.; He, B. Experimental Study on Rockburst of Granite With Prefabricated Folded Fissure Under True-Triaxial With Single Face Unloading. *J. Basic Sci. Eng.* **2025**, *33*, 1487–1503.
26. Yang, D.; Zhao, Y.; Teng, T.; Zhang, C.; Yang, J.; Yang, Z.; Liu, B. Study on Critical Characteristics of Acoustic Emission in Sandstone Fracture Instability and Kaiser Point Recognition. *J. Basic Sci. Eng.* **2021**, *29*, 218–230.
27. Zhang, Y.B.; Liang, P.; Sun, L.; Tian, B.; Yao, X.; Liu, X. Spectral characteristics of AE in the process of saturated granite fracture under uniaxial compression. *Rock Soil Mech.* **2019**, *40*, 2497–2506.
28. Wang, L.; Wang, L.; Xu, M.; Long, W. Damage evolution and destabilization precursors in granite under splitting load at different temperatures. *Trans. Nonferrous Met. Soc. China* **2024**, *34*, 977–994. [CrossRef]
29. Hou, Z.; Li, C.; Song, Z.; Xiao, Y.; Qiao, C.; Wang, Y. Investigation on Acoustic Emission Kaiser Effect and Frequency Spectrum Characteristics of Rock Joints Subjected to Multilevel Cyclic Shear Loads. *Geofluids* **2021**, *2021*, 5569525. [CrossRef]
30. Han, Q.; Yang, G.; Xu, J.; Fu, Z.; Lacidogna, G.; Carpinteri, A. Acoustic emission data analyses based on crumb rubber concrete beam bending tests. *Eng. Fract. Mech.* **2019**, *210*, 189–202. [CrossRef]
31. Vavryčuk, V. Inversion for parameters of tensile earthquakes. *J. Geophys. Res.* **2001**, *16*, 339–355. [CrossRef]

Disclaimer/Publisher's Note: The statements, opinions and data contained in all publications are solely those of the individual author(s) and contributor(s) and not of MDPI and/or the editor(s). MDPI and/or the editor(s) disclaim responsibility for any injury to people or property resulting from any ideas, methods, instructions or products referred to in the content.